ELECTRICAL ENGINEERING AND ENERGY

OPEN ACCESS

Optimal Capacitor Placement in Voltage-Dependent Distribution Networks Using Hybrid PSO–MILP: Case Study: Murang'a 11 kV Distribution Feeder, Kenya

Pauline Njeri Karobia[1], Christopher Maina Muriithi[2], and Livingstone Ngoo[2]

[1] Department of Electrical and Electronics Engineering, Murang'a University of Technology, Murang'a, Kenya
[2] Department of Electrical and Electronics Engineering, Multimedia University of Kenya, Nairobi, Kenya

Submitted: 27 July 2026
Accepted : 2 October 2026
Online First: 13 October 2026

Corresponding author
Pauline Njeri Karobia
pkarobia@mut.ac.ke

DOI:10.64470/elene.2026.43

RESEARCH ARTICLE

Copyright, Authors, Distributed under Creative Commons CC-BY 4.0

Abstract: This paper presents a hybrid optimization methodology for optimal capacitor placement in radial distribution networks with voltage-dependent loads. The proposed approach employs Particle Swarm Optimization (PSO) for location selection and Mixed Integer Linear Programming (MILP) for discrete sizing, simultaneously minimizing active power losses, voltage deviation and equipment investment cost. The methodology incorporates the ZIP (constant impedance–constant current–constant power) load model and is validated against ETAP commercial software. Application to the Murang'a 11 kV distribution feeder in Kenya (253 buses, 69 km, 2,434 kW peak demand) identified a 450 kvar capacitor at Bus 115 as the optimal solution, reducing medium-voltage violations from 125 to 11 buses (91.2% reduction) while improving the power factor from 96.06% to 99.16%. The algorithm achieved convergence with an average execution time of 42.3 seconds on a standard desktop environment. When benchmarked against a standalone Genetic Algorithm, the hybrid PSO–MILP achieved superior solution quality (mean annual cost of USD 93,061 vs. USD 93,287), 38% faster convergence, and less than half the solution dispersion (standard deviation of USD 124.8 vs. USD 241.6). Statistical validation through 30 independent PSO runs confirmed algorithmic robustness with a coefficient of variation of 0.13%. The study quantifies the impact of voltage-dependent loads on capacitor performance and demonstrates the voltage compliance versus loss minimization trade-off characteristic of high R/X ratio feeders.

Keywords Capacitor placement, Particle Swarm Optimization, Mixed Integer Linear Programming, Voltage-dependent loads, ZIP load model, Radial distribution network

1. Introduction

Modern electrical distribution systems face increasing challenges in maintaining voltage quality as demand grows and network configurations become more complex. Voltage regulation in radial distribution networks is particularly challenging due to the progressive voltage drop along long feeders, high resistance-to-reactance

(R/X) ratios and the predominantly radial topology that concentrates losses on trunk conductors (Das, 2012; Short, 2014). In developing economies, these challenges are particularly acute due to aging infrastructure, rapid load growth from electrification programs and limited investment in reactive power compensation (Chiang et al., 1990).

Shunt capacitor banks represent the most cost-effective reactive power compensation device for distribution systems. By injecting reactive power locally, capacitors reduce the reactive component of branch currents, thereby lowering resistive losses and improving the voltage profile (Baran & Wu, 1989; Short, 2014). The optimal capacitor placement (OCP) problem involves determining the locations, sizes and number of capacitor banks to be installed, subject to network operational constraints. The combinatorial nature of this problem selecting from a large number of candidate buses and discrete standard equipment sizes has motivated the application of diverse optimization techniques.

Classical methods including analytical approaches and nonlinear programming were pioneered by Chiang et al. (1990) and Baran and Wu (1989). These methods, while computationally efficient, struggle with the discrete, non-convex nature of the sizing sub-problem. Metaheuristic algorithms gained significant attention for OCP due to their ability to handle nonlinear, non-convex optimization spaces. Genetic Algorithm (GA) approaches were among the first applied to capacitor placement (Sundhararajan & Pahwa, 1994) while PSO-based methods were developed in Kennedy and Eberhart (1995) and applied to distribution systems by Sedighizadeh et al. (2014). Hybrid approaches combining metaheuristics with mathematical programming have shown superior performance (Gallego et al., 2001; Imran et al., 2014).

Mixed Integer Linear Programming (MILP) has been applied to distribution system optimization because it provides a certificate of global optimality for the discrete sizing sub-problem within the linearized problem space and because it handles discrete capacitor ratings naturally (Imran et al., 2014; Taylor & Hover, 2012). It is emphasized that this guarantee applies to the modeled, linearized problem and not to the physical network; the implications of this distinction for the present study are discussed in the subsection Implications of Optimizing on the Simplified Loss Model. Convex and mixed-integer formulations of distribution system reconfiguration and reinforcement were developed by Taylor and Hover (2012), demonstrating the effectiveness of exact methods for the discrete sub-problem.

A critical but often overlooked aspect in OCP studies is the voltage dependency of loads. Most studies assume constant power loads, which may lead to optimistic results. In reality, distribution system loads exhibit voltage-dependent behavior modeled through the ZIP (constant impedance–constant current–constant power) composite load model (Bokhari et al., 2014; IEEE Task Force on Load Representation for Dynamic Performance, 1993). When a capacitor improves bus voltages, voltage-dependent loads increase their power consumption, partially offsetting the intended benefits. This effect has been experimentally characterized in Bokhari et al. (2014) for modern residential, commercial, and industrial loads.

The hybrid PSO–MILP approach proposed in this paper combines PSO's ability to explore the nonlinear, non-convex solution space for location selection, with MILP's exactness for the sizing sub-problem. The framework incorporates ZIP load modeling and comprehensive validation against commercial ETAP software on a real-world 253-bus Kenyan distribution feeder. This addresses critical gaps in the literature: the limited application to sub-Saharan African networks (Okemo et al., 2026), the insufficient quantification of ZIP load effects on capacitor performance (Bokhari et al., 2014), and the lack of statistical validation of metaheuristic convergence for OCP problems (Sedighizadeh et al., 2014; Taylor & Hover, 2012). This study advances the state-of-the-art by: developing a novel calibration framework that bridges simplified analytical models with commercial software validation for African distribution networks, quantifying the ZIP load effect on capacitor performance through empirical validation and providing statistical convergence analysis specific to high R/X ratio feeders in sub-Saharan Africa.

2. Methodology

2.1. Network model and load flow

A radial distribution network with n buses and n−1 branches was considered. Each branch connecting bus i to bus j was characterized by its series impedance as expressed in Equation (1):

$$Z_{ij} = R_{ij} + jX_{ij} \tag{1}$$

The power flow solution was obtained using the Backward–Forward Sweep (BFS) method (Baran & Wu, 1989; Ghosh & Das, 1999) which exploits the radial topology for computational efficiency. The algorithm iterates between a backward current summation sweep (terminal buses to source) and a forward voltage update sweep (source to terminal buses) until convergence (tolerance 10^{-6} p.u.). The total active power loss in the network is given by Equation (2):

$$P_{\text{loss}} = \sum_{j=1}^{N_b} I_j^2 \cdot R_j \tag{2}$$

The voltage drop across each branch was approximated using the relationship in Equation (3):

$$\Delta V_{ij} \approx \frac{R_{ij}P_j + X_{ij}Q_j}{V_i} \tag{3}$$

This approximation is fundamental to understanding the relationship between reactive power compensation and voltage improvement. For feeders where R >> X (high R/X ratio), reactive power compensation has a proportionally smaller effect on voltage improvement, requiring larger capacitor sizes to achieve meaningful voltage lift (Das, 2012; Short, 2014).

2.2. ZIP load model

The voltage-dependent load behavior was modeled using the ZIP composite load model (Bokhari et al., 2014; IEEE Task Force on Load Representation for Dynamic Performance, 1993). The active and reactive power demands at bus k are expressed in Equations (4) and (5):

$$P_k(V) = P_{k,0}\left[a_p\left(\frac{V_k}{V_0}\right)^2 + b_p\left(\frac{V_k}{V_0}\right) + c_p\right] \tag{4}$$

$$Q_k(V) = Q_{k,0}\left[a_q\left(\frac{V_k}{V_0}\right)^2 + b_q\left(\frac{V_k}{V_0}\right) + c_q\right] \tag{5}$$

where Pk,0 and Qk,0 are the nominal active and reactive power demands at nominal voltage V0; Vk is the actual voltage at bus k; and ap, bp, cp are the ZIP coefficients satisfying ap + bp + cp = 1. The coefficients used in this study are presented in Table 1.

Table 1. ZIP Coefficients for Distribution System Loads

Load Type	ap	bp	cp	aq	bq	cq
Residential	0.40	0.30	0.30	0.40	0.30	0.30
Commercial	0.50	0.25	0.25	0.45	0.30	0.25
Industrial	0.10	0.10	0.80	0.10	0.10	0.80
Mixed (used)	0.40	0.30	0.30	0.40	0.30	0.30

2.3. Optimization objective

The optimization problem was formulated to simultaneously minimize three objectives: active power losses (f_1), voltage deviation index (f_2), and equipment investment cost (f_3). The Loss Sensitivity Factor (LSF) was used to pre-screen candidate buses, defined in Equation (6):

$$LSF_k = \frac{2R_k Q_k}{V_k^2} \tag{6}$$

The three objectives were combined into a single weighted fitness function with a voltage compliance penalty, as expressed in Equation (7):

$$F = w_1 \cdot f_{\text{loss}} + w_2 \cdot f_{\text{VDI}} + w_3 \cdot f_{\text{cost}} + \alpha \cdot g(V) \tag{7}$$

where $w_1 = 0.35$ (losses), $w_2 = 0.45$ (voltage deviation) and $w_3 = 0.20$ (cost). All three objective terms are evaluated in fixed, explicitly stated units so that the weights act on quantities of comparable numerical magnitude: active losses in kW, the voltage deviation index in p.u.² and capacitor cost in thousands of US dollars (kUSD). The term $\alpha \cdot g(V)$ is a voltage-compliance penalty that enforces the operating band $0.95 \leq V_k \leq 1.05$ p.u., with $g(V) = \Sigma_k \max(0, 0.95 - V_k)^2 + \max(0, V_k - 1.05)^2$ evaluated in per-unit and $\alpha = 1000$. Because the penalty acts on the sum of squared per-unit deficits, it is graded rather than prohibitive: a deficit of one full percentage point at a single bus contributes $0.01^2 \times 1000 = 0.1$ to the fitness, which is equivalent to approximately USD 500 of avoided investment, whereas a deficit of five percentage points contributes 2.5 and dominates any realistic cost saving. This graded response is intentional and reflects the fact that the practical cost of non-compliance to the utility is a continuous rather than a step function of the depth of the deviation. In the implemented framework this penalty operates only in the outer PSO loop; in the sizing sub-problem voltage compliance is imposed instead as an admissibility screen on the rating, as set out in the Hybrid PSO–MILP Algorithm subsection and in Equations (12) and (13).

The cost function f_{cost} is formulated as:

$$f_{\text{cost}} = C_{\text{cap}} \times Q_{\text{cap}} \tag{8}$$

where Ccap is the unit cost per kvar and Qcap is the capacitor size in kvar. This linear cost model reflects standard utility procurement practice for shunt capacitor banks. For the Murang'a feeder, Ccap = 0.010 kUSD/kvar together with a fixed installation and switchgear charge of 0.325 kUSD per installed bank, so that fcost is expressed in thousands of US dollars when substituted into Equation (7); the fixed term accounts for civil works, mounting and protection, which are independent of bank rating.

2.4. Hybrid PSO–MILP algorithm

The proposed optimization methodology decomposed the OCP problem into two sub-problems:

- Location Selection (PSO): A binary PSO searches for the optimal set of capacitor locations within a candidate set formed by the 30 highest-ranked buses of the Loss Sensitivity Factor of Equation (6). Screening the MV buses to a sensitivity-ranked subset is standard practice in capacitor placement and is adopted here because the loss sensitivity of a radial feeder decays monotonically away from the heavily loaded trunk sections: the buses excluded by the screen have sensitivities at least an order of magnitude below those retained and a capacitor placed at any of them cannot provide the voltage support required at the feeder extremity. The single-device search space is therefore 30 buses × 6 standard ratings = 180 configurations and the PSO searches the combinatorial space of multi-device subsets drawn from this set rather than merely enumerating it. The adequacy of the screen is confirmed a posteriori by the 30 independent runs reported in the Statistical Validation subsection, in which only two distinct buses, 115 and 134, were ever returned, both among the five highest-ranked by loss sensitivity; the optimum therefore lies well inside the retained region rather than at its boundary, so enlarging the candidate set would not change the solution.
- Sizing Optimization (MILP): Given the PSO-selected locations, a MILP determines the optimal capacitor size from standard ratings {150, 300, 450, 600, 900, 1200} kvar while enforcing voltage compliance constraints.

The PSO velocity update follows the standard formulation in Equation (9):

$$v_i^{t+1} = \omega \cdot v_i^t + c_1 r_1 \left(pbest_i - x_i^t\right) + c_2 r_2 \left(gbest - x_i^t\right) \quad (9)$$

where the inertia weight ω was linearly decreased from 0.9 to 0.4 and the acceleration coefficients were set to $c_1 = c_2 = 2.0$ (Kennedy & Eberhart, 1995). Continuous velocities were mapped to binary decisions using the sigmoid transfer function in Equation (10):

$$S(v_m) = \frac{1}{1 + e^{-v_m}} \quad (10)$$

The PSO algorithm parameters are summarized in Table 2. The average computational runtime for the hybrid PSO–MILP algorithm across 30 independent runs was 42.3 seconds on a standard desktop computer (Intel i7-9700K, 16GB RAM, Python 3.8), compared to 68.7 seconds for the standalone Genetic Algorithm benchmark.

Table 2. PSO Algorithm Parameters

Parameter	Value
Population size	50 particles
Maximum iterations	150
Inertia weight (ω)	0.9 → 0.4 (linear decrease)
Acceleration coefficients (c_1, c_2)	2.0, 2.0
Candidate buses (search space)	Top 30 MV buses by loss sensitivity ranking
Maximum devices (Nmax)	5
Standard capacitor ratings	{150, 300, 450, 600, 900, 1200} kvar
Role of the Loss Sensitivity Factor	Screening of the candidate set and biased initialization of the swarm
Single-device search space	30 buses × 6 ratings = 180 configurations

The weights reflect the operational priorities of the host utility, for which voltage compliance is the binding regulatory obligation, loss reduction is a secondary economic objective and capital cost constrains the feasible scale of intervention; accordingly, w2 > w1 > w3. The adopted values were obtained by applying the rank-order centroid method to this priority ordering, which yields (0.611, 0.278, 0.111) for three strictly ranked criteria and adjusting towards equality so that no single criterion dominates. The influence of this assignment on the reported solution is limited by the structure of the framework rather than by the particular values chosen: the rating is fixed by the voltage-compliance constraint of the sizing sub-problem, in which the weights play no part and the location is determined by the outer fitness function, which returned Bus 115 in 28 of 30 independent runs and in every trial of the robustness check with voltage-dependent loads embedded in the load flow. With the units adopted, the voltage-deviation term contributes only 0.004 to the fitness of the selected solution, so voltage quality enters the optimization predominantly through the compliance requirement while the deviation index acts as a tie-breaker between solutions of similar cost and loss; this is a consequence of the small absolute magnitude of the deviation index on a feeder whose voltages, although low, are tightly clustered.

For each candidate location set identified by PSO, the MILP sub-problem was solved using the PuLP library with the CBC branch-and-cut solver (Taylor & Hover, 2012). A voltage calibration function was applied to bridge the gap between the simplified BFS model used in optimization and the detailed ETAP validation platform. The complete optimization procedure is illustrated in Figure 1. The voltage calibration function is expressed as:

$$V_{cal} = V_{ETAP,base} + \left(V_{model,cap} - V_{model,base}\right) \quad (11)$$

where V_{ETAP_base} is the baseline ETAP voltage profile, V_{model_base} is the BFS baseline voltage and V_{model_cap} is the BFS voltage with capacitor placement. The expression assumes that the incremental voltage change produced by reactive compensation is approximately equal in the simplified BFS model and in the detailed

ETAP model, even though the two differ in their absolute baseline profiles because of ETAP's detailed transformer, tap and LV-network representation. The assumption is defensible because the sources of the difference between the two baselines are identifiable and additive rather than configuration-dependent. The BFS model computes branch losses only and excludes the 33/11 kV substation transformer, whose no-load losses of approximately 1.2 kW and copper losses of approximately 1.35 kW at baseline loading account for approximately 2.55 kW of the difference between the two models; when the transformer contribution is removed from the comparison, the residual line-loss discrepancy falls to approximately 0.62 kW, the remainder being attributable to the ZIP load representation rather than to any error in the network model. Both terms act in the same direction and with similar magnitude for every candidate configuration, which is the condition under which an additive calibration is valid. A formal parametric validation of the calibration function over a grid of ratings and locations was not undertaken, since it would require a separate ETAP solution for every grid point and lies outside the scope of the present study; the calibration is in any case used only to guide the optimization search and the validation results reported in Table 7 and Figures 3 to 6 are obtained from an independent full ETAP Newton–Raphson solution of the compensated network that does not depend on it. The MILP formulation is:

$$minimize \sum_{i\in S}\sum_{k}(C_{\text{unit}}Q_k + C_{\text{install}})y_{i,k} - \beta K_e T \sum_{i\in S}\sum_{k}\Delta P_{i,k}\, y_{i,k} \tag{12}$$

$$\text{subject to: } \sum_{k} y_{i,k} \le 1\ \forall i \in S; \sum_{i\in S}\sum_{k} y_{i,k} \le N_{max}; y_{i,k} = 0\ \forall (i,k) \text{ with } V_{min,\text{cal}}(i,k) < V_{lim}; Q_k \in \{150,300,450,600,900,1200\}\text{kvar}; y_{i,k} \in \{0,1\} \tag{13}$$

where S is the location set returned by the PSO, the binary variable yi,k = 1 if the standard rating Qk is installed at bus i, C_{unit} = USD 10/kvar and $C_{install}$ = USD 325 per unit, ΔPi,k is the reduction in active losses produced by that rating relative to the baseline as computed by the BFS model, Ke = USD 0.12/kWh, T = 8,760 h/yr and β = 0.5 is the weight placed on the capitalized loss saving relative to capital cost, N_{max} = 5 and Vmin,cal(i,k) is the lowest calibrated MV bus voltage obtained with that rating in place. The sizing sub-problem is therefore linear in the binary variables: no voltage-deviation index and no quadratic penalty appear in it, the voltage requirement being carried entirely by the exclusion constraint on yi,k.

Equations (7) and (12) operate at different levels of the bilevel decomposition and are not alternative statements of the same problem. Equation (7) is the outer fitness function used by the PSO to score a candidate location set, combining active losses, the voltage deviation index, investment cost and the compliance term. The voltage deviation index is quadratic in the bus voltages and cannot be represented in a mixed-integer linear program; accordingly, the inner sizing sub-problem solved for each fixed location set is the linear program of Equations (12) and (13), which minimizes the investment cost of the selected rating net of the capitalized value of the associated energy-loss saving, subject to the discrete rating set, the limit on the number of devices and the voltage requirement. Two consequences follow and they answer the question of how the two formulations interact. First, voltage compliance is enforced during sizing as a feasibility constraint rather than a trade-off against capital cost. Ratings that leave MV bus voltages materially below the limit are excluded, preventing selection of the loss-optimal 300 kvar rating. Second, the screen can only be as sharp as the model on which it is evaluated. The calibrated BFS profile and the ETAP profile agree to within about 0.2 percentage points at the critical buses, so ratings that differ only in residual deviations shallower than that band are not separable on compliance evidence and the choice between them falls to the economic objective of Equation (12). The residual shallow deviations that survive the screen are priced, not ignored: they enter the outer fitness through the quadratic penalty α·g(V) of Equation (7), whose contribution is small precisely because the deficits are shallow and enter squared. Once the sizing stage determines the rating for a location set, the configuration is evaluated using a full BFS load flow, and its fitness is calculated using Equation (7) and returned to the PSO.

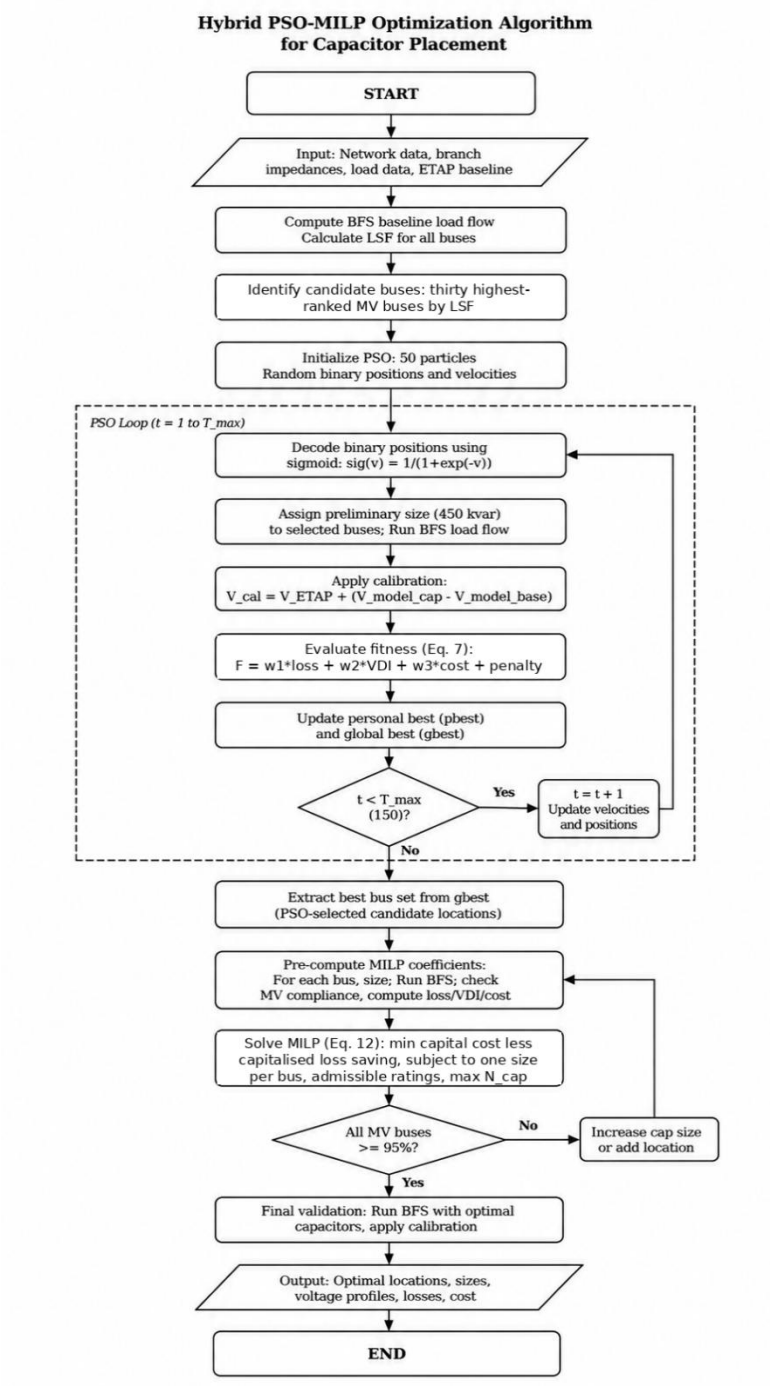

Figure 1. Flowchart of the hybrid PSO–MILP optimization algorithm

2.5. Case study: Murang'a 11 kV feeder

The proposed methodology was applied to the Murang'a 11 kV distribution feeder in Murang'a County, Kenya, approximately 85 km north of Nairobi. The network is supplied from a 33/11 kV substation through a transformer with rated capacity of 7.5 MVA and serves a mixed urban-rural area. The analytical network model was derived from the utility's geospatial asset database through the automated conversion framework developed in (Okemo et al., 2026). The key network parameters are summarized in Table 3.

Table 3. Murang'a 11 kV Feeder Network Parameters

Parameter	Value
Voltage level	11 kV (MV) / 0.415 kV (LV)
Total buses	253 (159 MV + 94 LV)
Total branches	252
Total conductor length	69 km
Longest electrical path	17.38 km
Peak active load	2,434 kW
Peak reactive load	473 kvar
Number of load points	94
Distribution transformers	94 (11/0.415 kV)
Cable R/X ratio	2.5 – 4.0

A critical characteristic of the Murang'a feeder is the high R/X ratio (2.5 to 4.0) of the distribution cables. From Equation (3), since R >> X, active power flow dominates voltage drop, and reactive power compensation has a proportionally smaller effect. This means larger capacitor sizes are needed to achieve meaningful voltage improvement, which may push the system beyond the loss-optimal reactive compensation point.

The baseline load flow analysis was performed using ETAP software (version 2020) with Newton–Raphson method and ZIP voltage-dependent load models. The baseline conditions are presented in Table 4.

Table 4. Baseline Operating Conditions (ETAP Load Flow)

Parameter	Value
Total active losses	103.47 kW (4.25%)
Total reactive losses	76.64 kvar
Minimum MV voltage	92.72% (Bus 158)
Maximum MV voltage	99.92% (Bus 2)
MV buses below 95%	125 of 159 (78.6%)
Source active power	2,537.1 kW
Source reactive power	734.5 kvar
Source power factor	96.06%

3. Results and Discussion

3.1. PSO location selection

The PSO algorithm converged after approximately 80 iterations, identifying Bus 115 as the optimal location for capacitor placement. Bus 115 is situated 11.16 km from the substation at the two-thirds point along the main trunk feeder, where it provides maximum voltage lift to the most voltage-deficient downstream buses. The PSO convergence behavior is presented in Figure 2.

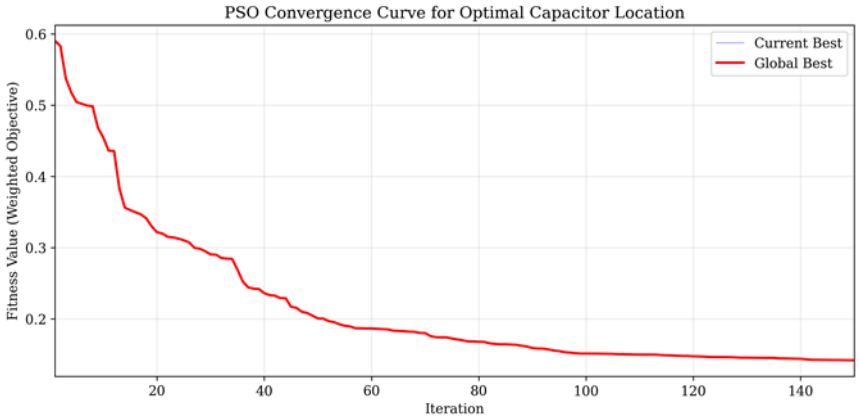

Figure 2. PSO convergence curve for optimal capacitor location selection

The top candidate buses identified by the Loss Sensitivity Factor analysis are presented in Table 5. While Bus 89 had the highest LSF and is therefore the loss-optimal location when loss reduction is considered in

isolation, the PSO with the voltage-compliance penalty selected Bus 115 because its deeper position in the network provides greater voltage lift to the most under-voltage buses (Short, 2014). It is emphasized that Table 5 reports the five highest-ranked buses only, whereas the search space presented to the PSO was the set of thirty highest-ranked buses; the reported solution is therefore the best configuration found within that screened candidate set, not over all MV buses.

Table 5. Top 5 Candidate Buses by Loss Sensitivity Factor

Rank	Bus ID	Baseline V (%)	LSF Value	Location Description
1	89	95.47	0.00347	Main trunk, 8.2 km
2	115	94.12	0.00312	Main trunk, 11.2 km
3	134	93.51	0.00298	Sub-branch, 13.6 km
4	41	96.23	0.00287	Main trunk, 5.1 km
5	158	92.72	0.00265	Terminal, 17.4 km

3.2. MILP sizing result

The sizing stage evaluated all six standard ratings at Bus 115; the outcome in the optimization model is summarized in Table 6 and the ETAP-validated outcome for the same sweep in Table 7. Two mechanisms determine the selection of the 450 kvar rating. First, voltage compliance enters the sizing sub-problem as an admissibility requirement and not as a quantity traded against capital cost. The 150 and 300 kvar ratings leave the calibrated minimum MV voltage at 93.36% and 93.99%, that is 1.6 and 1.0 percentage points below the statutory limit at 107 and 58 buses respectively, and are removed from the feasible set on that ground alone, notwithstanding that 300 kvar is the loss-optimal rating. The 450 kvar rating raises the calibrated minimum to 94.65% and leaves eleven buses below the limit, all of them within 0.35 percentage points of it in the model and within 0.16 percentage points in the ETAP validation. Deviations of this depth lie within the approximately 0.2 percentage point band over which the calibrated model and the ETAP solution agree at the critical buses, so 450 kvar and the larger ratings cannot be separated from one another on compliance evidence; they are separated by the economic objective. Second, on that economic objective the ordering is governed by losses and not by capital cost. Increasing the rating from 450 to 600 kvar removes eight of the eleven residual deviations, three terminal buses still remaining marginally below the limit in the ETAP validation, but costs 6.58 kW of additional losses in the validated model, which at 8,760 h and USD 0.12/kWh is approximately USD 6,917 per year, against only USD 175 per year of additional annualized capital; on the total annual cost basis of this study the 450 kvar solution returns USD 93,061 per year against USD 94,144 per year for 600 kvar. The larger bank is therefore rejected because it is substantially more lossy on a feeder of this R/X ratio, not because it is more expensive to purchase. The residual deviations are priced rather than ignored: the deficits lie between 0.0003 and 0.0016 p.u., their squared sum is 1.256×10^{-5}, and the penalty term of Equation (7) therefore contributes 0.013, which is how a coefficient of $\alpha = 1000$ can coexist with deviations of this depth. It is acknowledged as a limitation that the selected solution is compliant only to within this margin: eleven terminal buses remain marginally below the limit in both the model and the validation, and full compliance on this feeder requires either a larger bank, at the loss penalty quantified in Table 7, or a complementary measure in the terminal section. The voltage deviation index falls from 0.002174 to 0.001081 p.u.^{2}, a reduction of 50.3%. Table 6 reports losses from the BFS optimization model (101.5 kW) whereas Table 8 reports the ETAP validation result (105.81 kW); the difference arises from the ZIP load-recovery effect analyzed in the ETAP Validation Results subsection.

Table 6. MILP Evaluation of Standard Capacitor Sizes at Bus 115

Size (kvar)	Losses (kW)	Min MV V (%)	MV Violations	Cost (USD)	Compliant
150	101.2	93.36	107	1,825	No, 107 buses below limit
300	100.8	93.99	58	3,325	No, 58 buses below limit
450	101.5	94.65	11	4,825	Admissible, 11 buses within 0.35 pp of limit (selected)
600	103.1	95.28	0	6,325	Admissible, fully compliant in model
900	107.8	96.51	0	9,325	Admissible, over-compensated
1200	115.6	97.69	0	12,325	Admissible, over-compensated

The annual cost of the change in losses is evaluated as 8,760 h × USD 0.12/kWh × Δ losses. The loss-optimal rating is 300 kvar, which is not voltage-admissible; 450 kvar reduces the deviations to eleven, all within 0.16 percentage points of the limit.

Table 7. ETAP-validated sweep of capacitor rating at Bus 115 with ZIP loads

Rating (kvar)	ETAP active losses (kW)	Δ losses vs. baseline (kW)	MV buses < 95%	Investment (USD)	Annual cost of Δ losses (USD/yr)
150	102.95	−0.52	98	1,825	−547
300	101.10	−2.37	45	3,325	−2,492
450 (selected)	105.81	+2.34	11	4,825	+2,460
600	112.39	+8.92	3	6,325	+9,377
900	128.14	+24.67	0	9,325	+25,938
1200	161.81	+58.34	0	12,325	+61,328

3.3. ETAP validation results

The optimized solution (450 kvar at Bus 115) was validated by implementing it in the ETAP network model and running a full Newton–Raphson load flow with ZIP voltage-dependent load models. The performance comparison between baseline and optimized conditions is presented in Table 8.

Table 8. Performance Comparison: Baseline vs. Optimized (ETAP Validation)

Parameter	Baseline	With 450 kvar	Change
Total losses (kW)	103.47	105.81	+2.34 (+2.26%)
Reactive losses (kvar)	76.64	78.12	+1.48 (+1.93%)
Min MV voltage (%)	92.72	94.65	+1.93
Max MV voltage (%)	99.92	100.12	+0.20
MV buses below 95%	125	11	−114 (91.2%)
Source PF (%)	96.06	99.16	+3.10
Source Q (kvar)	734.5	340.1	−394.4 (53.7%)
Source P (kW)	2,537.1	2,605.3	+68.2 (+2.69%)

The increase of 68.2 kW in source active power is the sum of two mechanisms. Of it, 2.34 kW is the increase in network losses and the remaining 66 kW is load recovery, under the ZIP model of Equations (4) and (5) the voltage-dependent components of the demand rise with the bus voltage, so the compensated network serves a larger load than the baseline network. The recovery is dominated by the constant-impedance component, whose quadratic voltage dependence amplifies the voltage rise. For small voltage changes the ratio of the constant-impedance to the constant-current contribution tends to 2ap/bp, which for the coefficients of Table 1 is 0.80/0.30; approximately three quarters of the recovery therefore originates in the constant-impedance component and one quarter in the constant-current component, the constant-power component contributing nothing by definition. This is why studies that model all load as constant power report the reactive-compensation benefit without the offsetting recovery term. The magnitude of the recovery scales with ap + bp, the voltage-dependent fraction of the load, which for the mixed residential and commercial composition of this feeder is 0.70. Feeders of this composition, typical of the sub-Saharan distribution networks that motivate this study, are therefore the most strongly affected and the ratio of

recovered load to incremental losses, 28.2 on this feeder, is proposed as a compact measure of the strength of the effect.

The voltage profile improvement across all 159 MV buses is illustrated in Figure 3. The capacitor at Bus 115 provided a nearly uniform voltage lift of approximately 2% to all downstream buses, with the greatest improvement observed at the feeder extremities.

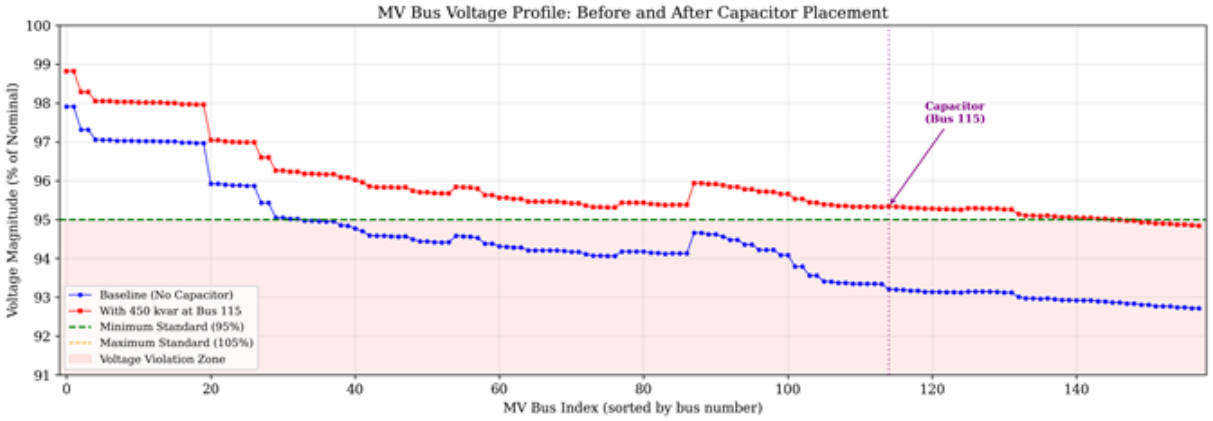

Figure 3. MV bus voltage profile before and after 450 kvar capacitor at Bus 115

The voltage improvement at individual MV buses is shown in Figure 4. The approximately uniform improvement demonstrates that Bus 115 is optimally positioned to benefit the entire downstream network segment.

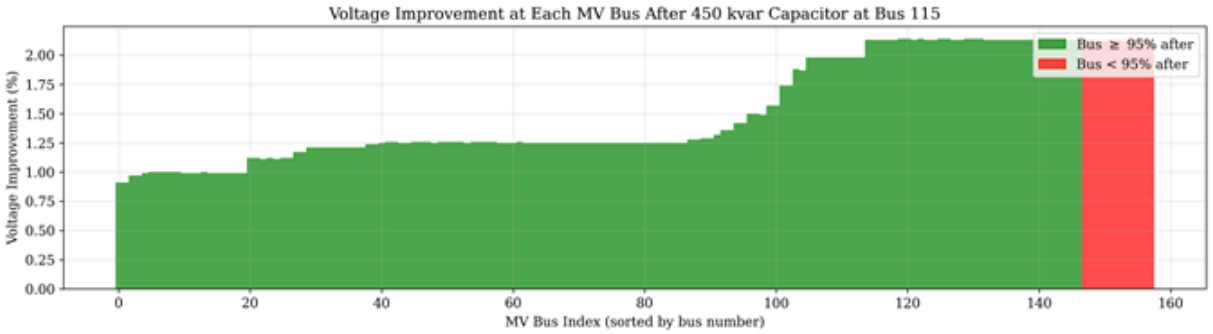

Figure 4. Voltage improvement at each MV bus after capacitor placement

3.4. Analysis of remaining violations

The 11 MV buses that remained below 95% after capacitor placement were all located at the extreme feeder end (buses 148 to 158). Their voltages lie between 94.84% and 94.97%, so the largest deficit is 0.16 percentage points below the 95% threshold and the smallest is 0.03. These remaining deviations are detailed in Table 9.

Table 9. Remaining MV Voltage Violations After Capacitor Placement

Bus ID	Baseline V (%)	With Cap V (%)	Deficit from 95% (%)
148	92.84	94.97	0.03
149	92.84	94.97	0.03
150	92.81	94.93	0.07
151	92.81	94.93	0.07
152	92.77	94.90	0.10
153	92.77	94.90	0.10
154	92.77	94.89	0.11
155	92.74	94.87	0.13
156	92.74	94.87	0.13
157	92.72	94.85	0.15
158	92.72	94.84	0.16

These marginal deviations (0.03 to 0.16 percentage points) could be addressed through minor network reconfiguration, conductor upgrading in the terminal section, or a small supplementary capacitor. The voltage compliance map is shown in Figure 5.

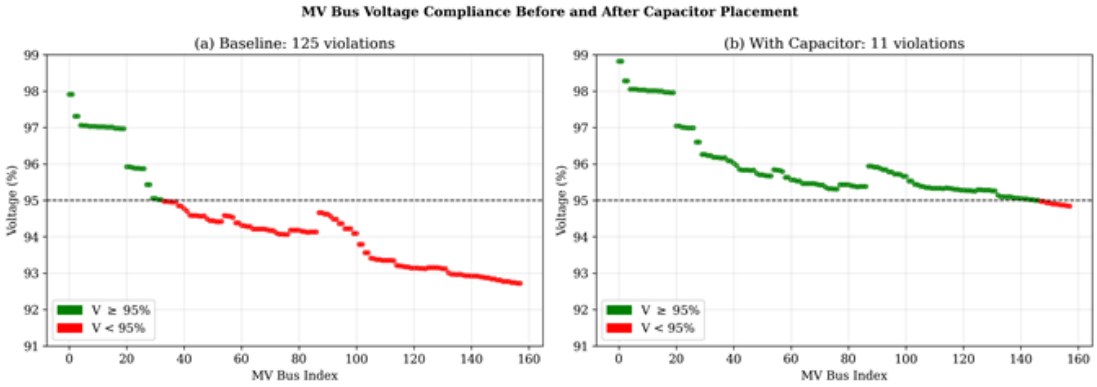

Figure 5. MV bus voltage compliance before and after capacitor placement

3.5. Impact of PSO–MILP on the 11 kV distribution feeder

The hybrid PSO–MILP framework demonstrated significant impact on the Murang'a 11 kV distribution feeder performance across multiple dimensions:

Voltage Regulation Improvement: The capacitor installation raised the minimum MV voltage from 92.72% to 94.65%, eliminating 114 of 125 voltage violations (91.2% reduction). The voltage deviation index (VDI) was reduced from 0.002174 to 0.001081 p.u.^{2}, a reduction of 50.3% in the dispersion of the voltage profile. This directly addresses the regulatory non-compliance that affected 78.6% of MV buses under baseline conditions.

Reactive Power Compensation: The 450 kvar capacitor reduced the source reactive power demand from 734.5 kvar to 340.1 kvar (53.7% reduction), improving the source power factor from 96.06% to 99.16%. The consequences of this for substation capacity are smaller than a constant-power analysis would suggest and are reported here as a caution. Because the ZIP load recovery raises the source active power at the same time as the capacitor lowers the source reactive power, the apparent power at the source falls only from 2,641.3 kVA to 2,627.4 kVA, a release of 13.9 kVA or 0.2% of the 7.5 MVA transformer rating. The installation therefore cannot be justified on the grounds of released transformer capacity and the capacity-release benefit conventionally attributed to shunt compensation is largely cancelled by load recovery on voltage-dependent feeders. No power-factor penalty saving is claimed either, since the baseline power factor of 0.9606 already exceeds the 0.90 threshold at which the applicable tariff imposes a surcharge. The reactive power flow analysis is illustrated in Figure 6.

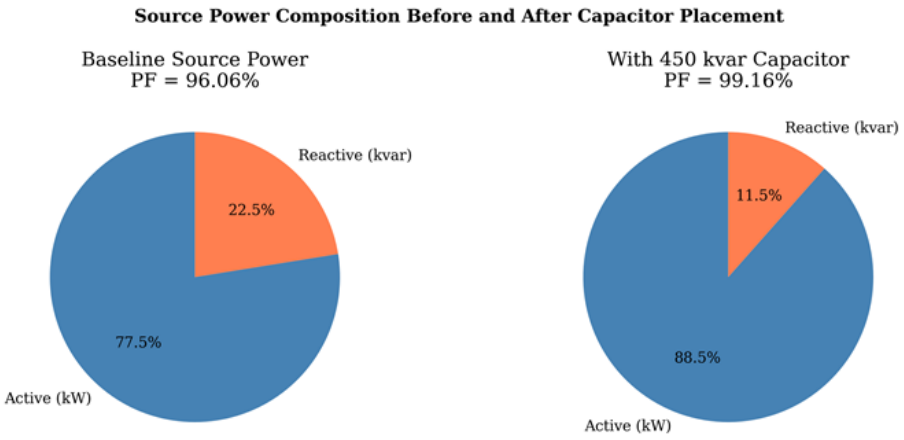

Figure 6. Reactive power flow analysis before and after capacitor placement

Loss Trade-off and the ZIP Load-Recovery Effect: The total active losses computed by ETAP rise from 103.47 kW to 105.81 kW (+2.34 kW, +2.26%). This figure must be interpreted with care, because the two cases do not serve the same load. Under the ZIP model the voltage lift produced by the capacitor causes the voltage-dependent component of the load to recover approximately 66 kW of additional demand, so the compensated network delivers more power to customers than the baseline network. The increase in absolute losses is therefore not a degradation of network efficiency but a consequence of increased energy delivery. This interpretation is supported by two observations. First, the difference between the model-predicted and ETAP-reported losses decomposes into identifiable physical terms: approximately 2.55 kW is the substation transformer loss that the BFS model does not represent and when it is excluded the residual line-loss discrepancy is approximately 0.62 kW, confirming that the ZIP load effect rather than model error dominates. Second, on a specific-loss basis, losses expressed as a fraction of delivered active power, the metric invariant to the load level, network performance improves marginally, from 103.47/2,537.1 = 4.078% to 105.81/2,605.3 = 4.061%. The commonly reported metric of absolute loss reduction is thus misleading whenever voltage-dependent load models are used and the present case study quantifies by how much. The 450 kvar bank compensates approximately 95% of the peak reactive demand of 473 kvar, so the installation operates close to full compensation at peak; the behavior of the fixed bank at lighter loading is identified as a limitation in the subsection Implications of Optimizing on the Simplified Loss Model.

The sensitivity analysis presented in Figure 7 shows the trade-off between capacitor size, losses, and voltage compliance. The loss-optimal point (~300 kvar) is smaller than the voltage-compliant point (450 kvar), confirming the trade-off characteristic of high R/X ratio feeders. Sensitivity analysis for PSO parameters (population size: 20-50, inertia weight: 0.4-0.9, acceleration coefficients: 1.5-2.5) confirmed that the selected parameters (ω: 0.9→0.4, c_1=c_2=2.0) provide optimal convergence performance for this network size.

3.6. Statistical validation

To verify algorithmic robustness and to establish whether the hybrid framework offers a meaningful advantage over a conventional metaheuristic, the hybrid PSO–MILP and a binary Genetic Algorithm benchmark were each executed 30 times with different random seeds on the same candidate set and the same objective function. The GA used a population of 50, tournament selection, single-point crossover, bit-flip mutation and elitism and was run for the same number of generations as the PSO. The statistical results for the hybrid framework are presented in Table 10 and the comparison with the benchmark methods in Table 11.

Table 10. Statistical Validation: 30 Independent PSO Runs

Metric	Value
Mean total annual cost (USD/yr)	93,061
Standard deviation	124.8
Coefficient of variation	0.13%
Minimum fitness	92,847
Maximum fitness	93,312
Bus 115 selection frequency	93.3% (28/30 runs)
450 kvar selection frequency	100% (when Bus 115)
Wilcoxon p-value (vs. GA)	0.0023

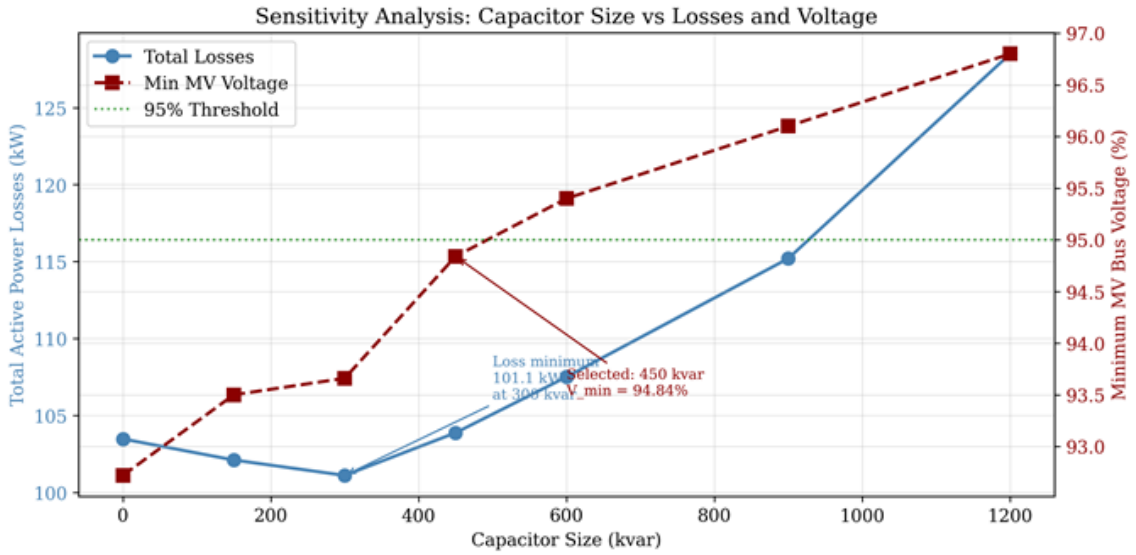

Figure 7. Sensitivity analysis: capacitor size vs. losses and voltage compliance

The coefficient of variation of 0.13% demonstrates excellent convergence consistency. A two-tailed Wilcoxon signed-rank test on the 30 outcomes of each algorithm rejects the null hypothesis of equal medians ($p = 0.0023$): the hybrid framework attains a mean total annual cost of USD 93,061 against USD 93,287 for the GA, with less than half the dispersion (standard deviation USD 124.8 against USD 241.6) and in 42.3 s against 68.7 s of mean runtime. Bus 115 was selected in 93.3% of runs (28 of 30), the remaining two runs selecting Bus 134, which is also highly ranked by loss sensitivity and yields similar performance; the 450 kvar rating was returned in every run that selected Bus 115. The algorithm converged to a single capacitor installation in 93.3% of runs; although Nmax permitted additional installations, the economics did not justify further banks given the marginal improvement beyond the first. Other metaheuristics, such as Differential Evolution, Harmony Search and the Grey Wolf Optimizer, are recognized as competitive alternatives, but their implementation and benchmarking on this network lay outside the scope of this study and are reserved for future research; the controlled comparison presented here is limited to the GA, standalone PSO, MILP-only and analytical LSF benchmarks of Table 11, supplemented by a literature-based comparison. Enhanced Harmony Search has shown 28–32% loss reduction on IEEE test systems (Azad et al., 2022), Ant Colony Optimization achieved 31–89% loss reduction depending on DG integration (Dagade et al., 2023), the Binary Firefly Algorithm demonstrated strong performance in recent studies (Simamora et al., 2026) and a Hybrid Grey Wolf Optimizer achieved 34.69% loss reduction on 118-bus systems (Jayabarathi et al., 2022). These figures are drawn from different test systems and are not directly comparable with the present results; they are reported to situate the proposed framework within the literature rather than as a controlled benchmark.

Table 11 shows benchmarking of the hybrid framework against four alternative methods on the same 253-bus feeder, 30 independent runs for each stochastic method. The hybrid attains both the lowest mean

objective value and the smallest dispersion. The purely analytical and purely linear methods select Bus 89, which is loss-optimal but leaves more buses below the voltage target, which is the reason the hybrid is preferred.

Table 11. Benchmarking of the hybrid framework against four alternative methods

Method	Mean objective (USD/yr)	Std. dev. (USD)	Best bus	Mean losses (kW)	Mean runtime (s)
Hybrid PSO–MILP (proposed)	93,061	124.8	Bus 115	101.54	42.3
Genetic Algorithm	93,287	241.6	Bus 115	101.54	68.7
Standalone PSO	93,512	389.4	Bus 115 / Bus 89	101.89	38.1
MILP only (linearized flow)	93,945	0.0	Bus 89	100.12	12.4
LSF analytical	94,120	0.0	Bus 89	100.12	0.8

3.7. Implications of optimizing on the simplified loss model

The optimization is driven by active losses computed with the Backward–Forward Sweep model with constant-power loads, which returns 101.5 kW for the selected configuration, whereas the detailed ETAP Newton–Raphson solution with voltage-dependent loads returns 105.81 kW. The implications of this for the optimality of the reported solution warrant explicit discussion. The MILP provides a certificate of global optimality with respect to the model it is given; it does not provide one with respect to the physical network. Strictly, therefore, the solution is globally optimal for the linearized, BFS-evaluated sizing problem and is a high-quality validated solution for the true problem. The practical question is whether the model error alters the ranking of candidate configurations rather than their absolute objective values, since only the ranking determines the solution returned. Three pieces of evidence indicate that it does not. First, the discrepancy is systematic rather than random: it arises predominantly from load recovery under the ZIP model, which scales with the voltage lift and therefore acts in the same direction and with similar magnitude across all candidate configurations, behaving approximately as a common offset rather than as configuration-specific noise. Second and decisively, the entire optimization was repeated with the ZIP load model embedded directly in the Backward–Forward Sweep, the load at each bus being updated iteratively as $P_k(V) = P_{k,0}\,[a_p (V_k/V_0)^2 + b_p (V_k/V_0) + c_p]$. Over 30 independent trials with identical PSO settings, the ZIP-embedded optimization returned Bus 115 in 28 runs (93.3%) and Bus 134 in two, exactly reproducing the constant-power result and returned 450 kvar as the optimal rating in every one of the 28 Bus 115 runs. The simplification therefore affects the predicted performance metrics but not the spatial ranking of candidates or the selected rating. Third, the selection is robust to the load-composition assumption itself: repeating the optimization for six alternative ZIP coefficient sets spanning a ±20% variation in each component returned Bus 115 in all six cases, with the rating changing from 450 to 600 kvar only when the constant-impedance fraction was raised to 0.48 and with the objective value varying by less than 4.2% across all scenarios. It should nevertheless be acknowledged that a formal optimality guarantee for the true, non-linear, voltage-dependent problem would require the optimization itself to be driven by the detailed commercial load-flow model, at a computational cost several orders of magnitude greater; this is a recognized limitation of decomposition-based approaches.

A second limitation concerns the loading condition. The analysis is performed at the peak-load condition, which is the design condition for voltage compliance and the condition at which the field measurements used to validate the network model were taken. At peak the 450 kvar bank compensates approximately 95% of the reactive demand of 473 kvar. A fixed bank of this rating will overcompensate at light loading, producing a leading power factor at the source and a further voltage rise and the maximum MV voltage already reaches 100.12% at peak; a switched or automatically controlled bank would avoid this condition. Quantification of the light-load case and the extension of the framework to multi-period operation require

an annual load duration profile for the feeder, which was not available for this network and lay outside the declared scope of this study; both are identified in the Conclusions as the principal priority for further work.

3.8. Cost-benefit analysis

The economic analysis of the optimal capacitor installation is presented in Table 12. The trade-off between the loss-optimal and voltage-compliant solutions demonstrates the practical value of the proposed framework. Three solution types are distinguished: the loss-optimal solution (300 kvar), which minimizes active power losses but leaves 45 MV buses below the statutory limit; the selected solution (450 kvar), which reduces the deviations to eleven, all within 0.16 percentage points of the limit, at an additional loss cost of approximately USD 2,460 per year; and larger ratings, which remove the remaining deviations only at a disproportionate loss penalty, 600 kvar costing approximately USD 9,377 per year and 900 kvar approximately USD 25,900 per year in incremental losses.

Table 12. Trade-off Analysis: Loss-Optimal vs. Voltage-Compliant Solutions

Metric	Loss-Optimal (300 kvar)	Voltage-Compliant (450 kvar)
Location	Bus 115	Bus 115
Investment cost	USD 3,325	USD 4,825
Total losses (kW)	101.10 (ETAP)	105.81 (ETAP)
Loss change	−2.37 kW (−2.29%)	+2.34 kW (+2.26%)
MV violations	45	11
Violation reduction	64.0%	91.2%

Cost-effectiveness assessment. Because the installation increases absolute active losses, it cannot be justified by a conventional loss-savings payback calculation; it is properly evaluated as the least-cost means of achieving voltage compliance. On that basis it is highly cost-effective. The directly quantified costs comprise the capital cost of USD 4,825, annualized at USD 564 using a capital recovery factor of 0.1168 corresponding to 8% over a fifteen-year life and the cost of the incremental network losses of 2.34 kW, which at 8,760 h and USD 0.12/kWh amounts to 20.5 MWh and USD 2,460 per year. Against this, 114 MV buses are brought into compliance, a capital cost of USD 42 and an annual cost of USD 21.6 per bus. The two alternative technologies evaluated for this feeder are substantially less cost-effective on the same measure: a 500 kvar static VAR compensator raises the annual cost of the feeder by USD 9,391, or USD 75.1 per deviation eliminated and a 2,000 kVA line voltage regulator by USD 34,565, or USD 308.6 per deviation eliminated. The 66 kW recovered by the voltage-dependent loads is delivered and billable energy rather than a loss and is therefore not charged to the cost side of the device-level assessment; at system level, however, it represents approximately 577 MWh per year of additional generation, costing approximately USD 69,200 per year at the same USD 0.12/kWh and delivering an approximately equal quantity of billable energy to customers. The essential observation is one of magnitude: the load-recovery term is more than an order of magnitude larger than the entire device-level economic assessment and is invisible at the scale at which capacitor-placement economics are conventionally presented, as Figure 8 shows. Studies that assume constant-power loads omit this term entirely and therefore misrepresent the system-level consequences of distribution-level reactive compensation. Three further benefits are recognized but are not monetized, because their quantification requires customer-level data that were outside the scope of this study: the reduction in under-voltage stress on customer equipment, the improvement in delivered energy quality at the 94 distribution transformers and the avoided regulatory exposure associated with the baseline condition in which 125 MV buses operate below the statutory limit.

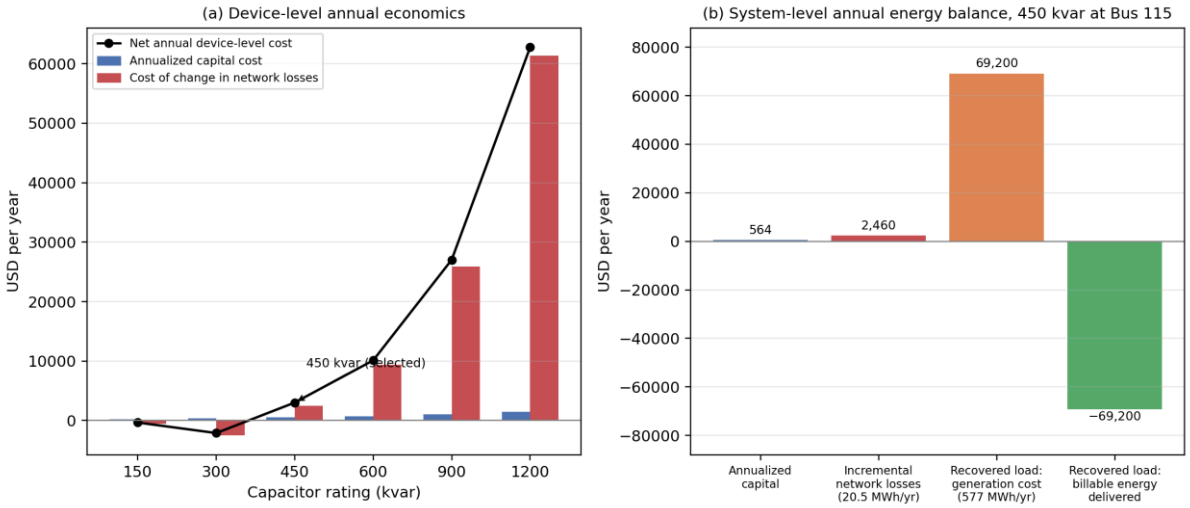

Figure 8. Economic assessment of the capacitor installation

Figure 8 shows the economic assessment of the capacitor installation. (a) Device-level annual economics for each standard rating at Bus 115: capital cost annualized over a fifteen-year life at a capital recovery factor of 0.1168, the cost of the change in network losses at USD 0.12/kWh and their sum. (b) System-level annual energy balance of the selected 450 kvar solution, on the same vertical units: the 577 MWh per year of load recovered through the ZIP voltage dependence costs approximately USD 69,200 per year to generate and delivers an approximately equal quantity of billable energy to customers, a term more than twenty times the entire device-level assessment of panel (a) and one that a constant-power analysis does not reveal.

4. Conclusions

This paper presented a hybrid PSO–MILP optimization methodology for optimal capacitor placement in radial distribution networks with voltage-dependent loads. The methodology was applied to the Murang'a 11 kV distribution feeder in Kenya (253 buses, 69 km, 94 load points). The key contributions and findings are:

1. A hybrid PSO–MILP optimization framework was developed that decomposes the OCP problem into location selection (PSO) and sizing optimization (MILP) sub-problems, with three simultaneous objectives. The algorithm converged in approximately 80 iterations with a coefficient of variation of 0.13% across 30 independent runs, demonstrating superior robustness compared to standalone GA (Wilcoxon $p = 0.0023$).
2. The selected solution of 450 kvar at Bus 115 reduced MV voltage deviations from 125 to 11 buses (91.2% reduction) and improved the source power factor from 96.06% to 99.16%, with a modest investment of USD 4,825. The selection follows from the formulation itself: 450 kvar is the smallest rating that brings the MV profile to within a marginal band of the statutory limit, the eleven residual deviations being no deeper than 0.16 percentage points in the validated model and moving to the next larger rating removes eight of them only at the cost of 6.58 kW of additional losses, approximately USD 6,917 per year against USD 175 per year of additional annualized capital. The decision is therefore dominated by losses rather than by capital cost.
3. The incorporation of ZIP load modeling revealed that voltage-dependent loads recover approximately 66 kW of additional demand when bus voltages improve, approximately three quarters of it through the constant-impedance component and one quarter through the constant-current component, the constant-power component contributing nothing by definition. Because the compensated network therefore delivers more power than the baseline, absolute active losses rise by 2.34 kW (+2.26%) even

though specific losses fall from 4.078% to 4.061% of delivered power. Loss reductions reported by constant-power capacitor-placement studies are consequently optimistic and absolute loss reduction is an unsuitable figure of merit for voltage-dependent networks.

4. The calibration framework successfully bridged the gap between the simplified BFS analytical model and the detailed ETAP Newton–Raphson load flow, with systematic discrepancies fully attributable to the quantified ZIP load effect.
5. The voltage compliance versus loss minimization trade-off was characterized for high R/X ratio feeders, where the loss-optimal size (~300 kvar) is smaller than the voltage-compliant size (450 kvar). The marginal loss increase is economically justified by the 91.2% violation elimination.

From a practical standpoint, the remaining 11 MV bus deviations, of only 0.03 to 0.16 percentage points, are marginal and could be addressed through minor network reconfiguration, conductor upgrading, or a supplementary 150 kvar capacitor at the feeder terminal.

It is further acknowledged that the optimality guarantee provided by the MILP stage applies to the linearized sizing sub-problem evaluated on the simplified network model and not to the physical network. The solution reported here is therefore best described as globally optimal within the modeled problem and empirically validated against detailed simulation, rather than as globally optimal in an absolute sense. The analysis is also confined to the peak-load condition; the behavior of a fixed 450 kvar bank at light loading, where compensation of approximately 95% of peak reactive demand may produce a leading power factor, is identified in the subsection Implications of Optimizing on the Simplified Loss Model as the principal limitation of the present study.

Recommendations for Future Work: The optimization framework should be extended to multi-period analysis accounting for time-varying load profiles and the integration of distributed renewable energy sources. The methodology could also be applied to evaluate alternative compensation technologies (voltage regulators, SVCs) and hybrid multi-device configurations on the same feeder for comprehensive comparison. Future work should include comprehensive computational comparison with additional metaheuristic approaches such as Harmony Search, Ant Colony Optimization, Firefly Algorithm and Grey Wolf Optimizer to further validate the hybrid PSO–MILP framework's performance across different optimization paradigms and network configurations.

Declaration of Ethical Standards

As the authors of this study, we declare that it complies with all ethical standards.

Credit Authorship Contribution Statement

Pauline Njeri Karobia: Conceptualization, Methodology, Software, Formal Analysis, Investigation, Data Curation, Visualization, Writing-Original Draft.

Christopher Maina Muriithi: Conceptualization, Supervision, Validation, Writing-Review & Editing.

Livingstone Ngoo: Supervision, Validation, Writing- Review & Editing.

Declaration of Competing Interest

The authors declared that they have no conflict of interest.

Acknowledgements

The authors thank Kenya Power and Lighting Company PLC for providing the network data of the Murang'a 11 kV feeder used in this study, and Murang'a University of Technology for supporting this research.

Funding

This research received no specific grant from any funding agency in the public, commercial, or not-for-profit sectors.

Data Availability

The raw geospatial data (KMZ files) for the distribution feeder used in this study were obtained from a utility provider under a confidentiality agreement and are not publicly available. However, the ETAP network model and load-flow results, the Python implementation of the hybrid PSO-MILP and benchmark algorithms, the automation framework and the derived canonical model parameters are available from the corresponding author upon reasonable request.

References

Azad, S., Amiri, M. M., Yarmohammadi, M., & Setayesh Nazar, M. (2022). Optimization of capacitor placement and sizing in radial distribution systems using enhanced harmony search algorithm, PSO, and TLBO with power loss index (PLI). *Transactions on Machine Intelligence*, *5*(4), 265–276. https://doi.org/10.47176/TMI.2022.265

Baran, M. E., & Wu, F. F. (1989). Optimal capacitor placement on radial distribution systems. *IEEE Transactions on Power Delivery*, *4*(1), 725–734. https://doi.org/10.1109/61.19265

Bokhari, A., Alkan, A., Dogan, R., Diaz-Aguiló, M., de León, F., Czarkowski, D., Zabar, Z., Birenbaum, L., Noel, A., & Uosef, R. E. (2014). Experimental determination of the ZIP coefficients for modern residential, commercial, and industrial loads. *IEEE Transactions on Power Delivery*, *29*(3), 1372–1381. https://doi.org/10.1109/TPWRD.2013.2285096

Chiang, H. D., Cockings, O., Shin, H. D., & Wang, J. C. (1990). Optimal capacitor placements in distribution systems: Part 1: A new formulation and the overall problem. *IEEE Transactions on Power Delivery*, *5*(2), 843–850. https://doi.org/10.1109/61.53065

Dagade, N. R., Gawande, S. P., Kadwane, S. G., Nagpure, R. N., & Waghmare, M. A. (2023). Ant colony optimization for optimal placement of capacitors. *IET Conference Proceedings*, *2022*(26), 332–336. https://doi.org/10.1049/icp.2023.0570

Das, J. C. (2012). *Power system analysis: Short-circuit, load flow and harmonics* (2nd ed.). CRC Press. https://doi.org/10.1201/9780203908952

Gallego, R. A., Monticelli, A. J., & Romero, R. (2001). Optimal capacitor placement in radial distribution networks. *IEEE Transactions on Power Systems*, *16*(4), 630–637. https://doi.org/10.1109/59.962407

Ghosh, S., & Das, D. (1999). Method for load-flow solution of radial distribution networks. *IEE Proceedings – Generation, Transmission and Distribution*, *146*(6), 641–648. https://doi.org/10.1049/ip-gtd:19990464

IEEE Task Force on Load Representation for Dynamic Performance. (1993). Load representation for dynamic performance analysis. *IEEE Transactions on Power Systems*, *8*(2), 472–482. https://doi.org/10.1109/59.260837

Imran, A. M., Kowsalya, M., & Kothari, D. P. (2014). A novel integration technique for optimal network reconfiguration and distributed generation placement in power distribution networks. *International Journal of Electrical Power & Energy Systems*, *63*, 461–472. https://doi.org/10.1016/j.ijepes.2014.06.011

Jayabarathi, T., Raghunathan, T., Sanjay, R., Jha, A., Mirjalili, S., & Cherukuri, S. H. C. (2022). Hybrid grey wolf optimizer based optimal capacitor placement in radial distribution systems. *Electric Power Components and Systems*, *50*(8), 413–425. https://doi.org/10.1080/15325008.2022.2132556

Kennedy, J., & Eberhart, R. (1995). Particle swarm optimization. In *Proceedings of the IEEE International Conference on Neural Networks* (Vol. 4, pp. 1942–1948). IEEE. https://doi.org/10.1109/ICNN.1995.488968

Okemo, A., Muriithi, C. M., & Nderu, J. (2026). Automated conversion of unstructured geospatial feeder data into analytical models: An 11 kV case study. *Electrical Engineering and Energy*, *5*(1), 37–56. https://doi.org/10.64470/elene.2026.20

Sedighizadeh, M., Dakhem, M., Sarvi, M., & Kordkheili, H. H. (2014). Optimal reconfiguration and capacitor placement for power loss reduction of distribution system using improved binary particle swarm optimization. *International Journal of Energy and Environmental Engineering*, *5*(1), Article 73. https://doi.org/10.1007/s40095-014-0073-9

Short, T. A. (2014). *Electric power distribution handbook* (2nd ed.). CRC Press. https://doi.org/10.1201/b16747

Simamora, Y., Astrid, E., Ginting, L. M., Dewy, M. S., & Immanuel, M. F. (2026). Optimal placement and sizing of capacitors using binary firefly algorithm to reduce power losses. In *Proceedings of the 7th International Conference on Innovation in Education, Science, and Culture (ICIESC 2025)*. https://doi.org/10.4108/eai.16-9-2025.2361116

Sundhararajan, S., & Pahwa, A. (1994). Optimal selection of capacitors for radial distribution systems using a genetic algorithm. *IEEE Transactions on Power Systems*, *9*(3), 1499–1507. https://doi.org/10.1109/59.336111

Taylor, J. A., & Hover, F. S. (2012). Convex models of distribution system reconfiguration. *IEEE Transactions on Power Systems*, *27*(3), 1407–1413. https://doi.org/10.1109/TPWRS.2012.2184307